Solvent Protection of the Hammerhead Ribozyme in the Ground State: Evidence for a Cation-Assisted Conformational Change Leading to Catalysis†

Ken J. Hampel and John M. Burke*

Department of Microbiology and Molecular Genetics, The Markey Center for Molecular Genetics, The University of Vermont, Burlington, Vermont 05405

Received November 18, 2002; Revised Manuscript Received February 13, 2003

ABSTRACT: Tertiary folding of the hammerhead ribozyme has been analyzed by hydroxyl radical footprinting. Three hammerhead constructs with distinct noncore sequences, connectivities, and catalytic properties show identical protection patterns, in which conserved core residues (G5, A6, U7, G8, and A9) and the cleavage site (C17, G1.1, and U1.2) become reproducibly protected from nucleolytic attack by radicals. Metal ion titrations show that all protections appear together, suggesting a single folding event to a common tertiary structure, rather than an ensemble of different folds. The apparent binding constants for folding and catalysis by Mg^{2+} are lower than those for Li^{+} by 3 orders of magnitude, but in each case the protected sites are identical. For both Mg^{2+} and Li^{+}, the ribozyme folds into the protected tertiary structure at significantly lower cation concentrations than those required for cleavage. The sites of protection include all of the sites of reduced solvent accessibility calculated from two different crystal structures, including both core and noncore nucleotides. In addition, experimentally observed protected sites include additional sequences adjacent to those predicted by the crystal structures, suggesting that the solution structure may be folded into a more compact shape. A 2′-deoxy substitution at G5 abolishes all protection, indicating that the 2′-OH is essential for folding. Together, these results support a model in which low concentrations of metal ions fold the ribozyme into a stable ground state tertiary structure that is similar to the crystallographic structures, and higher concentrations of metal ions support a transient conformational change into the transition state for catalysis. These data do not themselves address the issue as to whether a large- or small-scale conformational change is required for catalysis.

Ribozymes are convenient systems with which to study RNA[1] folding, since catalytic activity reports on their native folding. The hammerhead ribozyme is a small, conserved catalytic motif that exists in nature in plant viroids (*1*), viriod-like satellite RNA, and some eukaryotic species (*2*−*4*). In addition, it is a common self-cleaving RNA motif that can be isolated from random sequences by in vitro selection (*5*). Thus, the ribozyme motif appears to represent a simple, efficient biological strategy for effecting site-specific RNA cleavage. The transesterification reaction is initiated by a nucleophilic attack of the 2′-oxygen of the nucleotide 5′ to the cleavage site, residue C17, on the cleavage site phosphorus, yielding a 2′,3′-cyclic phosphate and 5′-hydroxyl products (*6*, *7*). On the basis of the observation that for all well-studied hammerheads the cleavage rate increases with pH in a log-linear relationship, the rate-limiting step for catalysis by the hammerhead is postulated to be the chemistry of the reaction (*8*−*10*). It has also been suggested, however, on the basis of recent crystallographic data, that a pH-dependent conformational change localized at the active site may be rate limiting (*11*). Indeed, the bulk of the current evidence cannot rule out either possibility.

The hammerhead motif adheres to a conserved three-way helical junction secondary structure where the helical elements may vary in sequence, but the identities of bases at the junction of the three helices are critical for activity (*6*, *7*, *12*). A domain organization has been described and is based on the tertiary folding observed in the X-ray structures of Scott, McKay, and co-workers (*13*, *14*). Stems 2 and 3 are coaxially stacked on one another with stem 2 extended toward stem 3 by noncanonical base pairs (Figure 1). This motif comprises domain 2. Domain 1 is structurally homologous to the U-turn motif in the anticodon and pseudouridine loops of yeast $tRNA^{Phe}$ and comprises the first four residues 3′ to stem 1, C3−A6. The global fold of the ribozyme resembles a y-shape with stems 2 and 3 stacked and stems 1 and 2 subtended by an acute angle. Domain 1 is bulged out toward stem 3 with a putative contact between the 2′-hydroxyls of G5 and residue 15.2.

A number of chemical and biophysical methods have been employed to confirm this specific geometry and to study cation-assisted folding of the ribozyme (*15*−*19*). FRET analysis has been employed to define the angles between all three helical axes (*16*). Metal ion titrations using the FRET signals as the assay demonstrated that folding to the y-shape

† This work was supported by NIH Grant GM65552 to J.M.B.

* To whom correspondence should be addressed. Phone: 802-656-8503. Fax: 802-656-5172. E-mail: john.burke@uvm.edu.

[1] Abbreviations: RNA, ribonucleic acid; DNA, deoxyribonucleic acid; FRET, fluorescence resonance energy transfer; trFRET, time-resolved fluorescence resonance energy transfer; TEB, transient electric birefringence; NMR, nuclear magnetic resonance; ATP, adenosine 5′-triphosphate; rpm, revolutions per minute; MES, 2-(*N*-morpholino)-ethanesulfonic acid; Tris, tris(hydroxymethyl)aminomethane; EDTA, ethylenediaminetetraacetic acid.

10.1021/bi020659c CCC: $25.00
Published on Web 03/28/2003

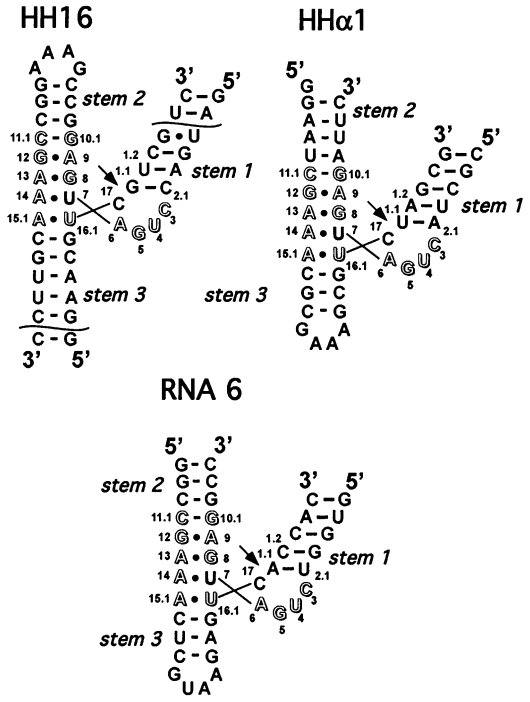

FIGURE 1: Secondary structures of the ribozyme constructs used in this study. These representations emphasize the global geometry of the ribozyme as seen in all crystal structures. Base numbering is according to Hertel et al. (*57*). Outlined letters indicate essential core nucleotides. An arrow marks the site of cleavage. For the initial footprinting experiments a shortened version of the HH16 ribozyme (*42*) was employed. Markings on stems 1 and 2 indicate the truncation of that construct. Cleavage kinetics and cation dependence footprinting were carried out with the full-length version of HH16. HHα1 was previously characterized by Clouet-d'Orval and Uhlenbeck (*43*), and RNA 6 has been employed for crystallographic studies by the Scott laboratory (*44*).

occurs with two discrete transitions (*16*). At submillimolar concentrations of Mg^{2+} the domain 2 stack is formed, and at low millimolar concentrations the domain 1 motif takes on a specific structure which orients stem 1 in close proximity with stem 2. Ribose 2′-deoxy substitution of G5, a conserved domain 1 residue (*20*), alters the geometry of the three-way junction such that stems 1 and 2 are not closely juxtaposed while maintaining the domain 2 structure (*21*). This substitution provides evidence for a partially structured intermediate, thus substantiating the proposal for a folding pathway.

Cations are required for folding to the specific global structure described above. In most studies divalent cations, principally Mg^{2+}, have been employed to study folding. Catalysis, however, can employ a broad range of cations. Divalent cations including Mg^{2+}, Mn^{2+}, Ca^{2+}, and Sr^{2+} (*22*), monovalents Na^+, NH_4^+, and Li^+ (*23*−*25*), and the multivalent cation cobalt(III) hexaammine (*24*) are all capable of promoting some level of hammerhead cleavage. This has led to the conclusion that catalysis does not have an absolute requirement for divalent metal ions or for inner-sphere coordination (*23*, *24*). However, some rate enhancement by divalent metal ions has been observed (*25*). In addition, it has been suggested that the apparent K_d^{Mg} for folding is lower than that for catalysis (*26*). This suggests that one or more divalent ions may be required to promote a change in the structure of the ground state toward the transition state. A large-scale conformational change from the geometry observed in the crystal forms has also been postulated to lead to the transition state (*27*).

Since global folding does not appear to be rate limiting for catalysis, it is not possible to study folding by studying the catalytic rate, an approach that has been valuable for investigating the folding of the *Tetrahymena* group I intron folding pathway (*28*). Although methods such as FRET (*16*), cross-linking (*29*, *30*), transient electric birefringence (TEB) (*19*), and 2-aminopurine fluorescence assays (*26*) are able to provide important global and local folding data, there is a need for methods that can probe the structure of the entire hammerhead motif and mutants with diminished catalytic activity at the resolution of individual nucleotides. Chemical footprinting methods have been widely utilized to study equilibrium and kinetic folding of RNA, DNA, and protein−nucleic acid complexes (*31*−*35*). The main benefit of these methods is the ability to monitor the chemical accessibility at nucleotide resolution for the entire molecule in a single experiment. Hydroxyl radical footprinting has been used to study the solvent accessibility of the C4′ atom of ribose residues in RNA (*36*), and we have recently used this approach to examine the structure and folding of the hairpin ribozyme (*37*, *38*). The method allows us to study the structural consequences of base change and functional group substitutions in comparison to changes in the catalytic potential of mutants. Here we report on a cation-dependent folding transition in the hammerhead ribozyme revealed by hydroxyl radical footprinting.

MATERIALS AND METHODS

Materials. All chemicals used in this study were of reagent grade or better. RNA was purchased from Dharmacon and deprotected according to the manufacturer's instructions or synthesized by standard phosphoramidite chemistry and deprotected as described previously (*39*). Oligonucleotides were purified by electrophoresis through 8 M urea−polyacrylamide gels as previously reported (*40*). Radiolabeled RNAs were prepared by phosphorylation of the 5′-terminal hydroxyl group with [γ-^{32}P]ATP and T4 polynucleotide kinase.

Footprinting Assays. For footprinting under equilibrium conditions, an 8 μL solution containing 5′-^{32}P-end-labeled RNA, a saturating concentration of unlabeled RNA (HH16, 1 μM; HHα1 and RNA 6 and 5 μM), 25 mM sodium cacodylate, pH 7, and cation was combined and incubated at 37 °C for 20 min. This solution were allowed to equilibrate to 25 °C and then treated with 0.7 μL each of 0.35% (v/v) H_2O_2 [freshly prepared from a 30% (v/v) stock solution], 60 mM sodium ascorbate (60 mM stocks can be stored at −20 °C), and Fe(II)-EDTA [5 mM EDTA, 5 mM $Fe(NH_4)_2(SO_4)_2$, mixed immediately prior to experiment] to give a final volume of 10 μL and the final concentration of cation shown in each figure. Concentrations of EDTA and Fe(II) were reduced compared to previously published methods to limit the concentration of free EDTA which could chelate Mg^{2+} in titration experiments. The RNA−cation solution was treated with reagents for 2 min and then quenched by adding 2 volumes of gel addition buffer [95% (v/v) formamide, 20 mM EDTA, 0.02% (w/v) bromophenol blue, 0.02% (w/v) xylene cyanol, 10 mM thiourea and 0.5 μg of tRNA] for

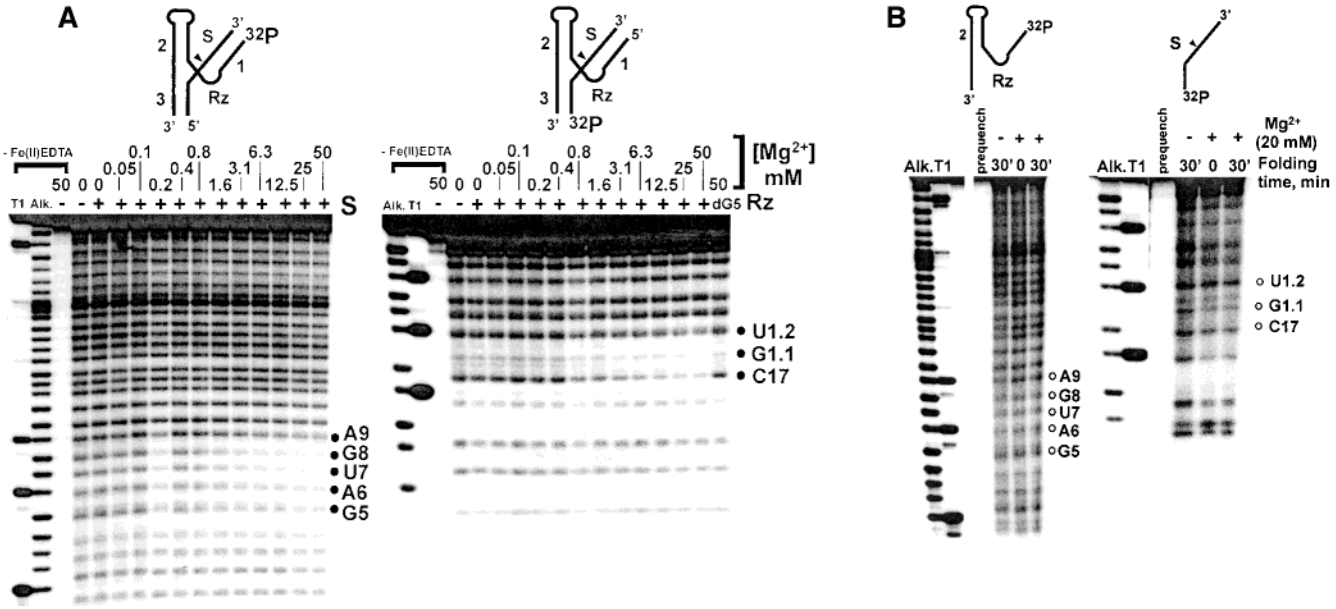

FIGURE 2: Solvent protection of ribose moieties is induced by tertiary folding in Mg^{2+} solutions. (A) Hydroxyl radical probing of ribozyme−substrate complexes in the presence of varying concentrations of Mg^{2+}. (B) Negative control experiments demonstrating that ribozyme and substrate strands alone do not form solvent-protected pockets in Mg^{2+} even after prolonged incubation. Reactions were carried out in 25 mM sodium cacodylate, pH 7.1, at the Mg^{2+} concentrations shown with or without saturating unlabeled ribozyme (Rz) or substrate (S) strands. Stick diagrams of the constructs showing the labeled strand are shown above each panel. RNAs were separated on 15% v/w (for labeled Rz) and 20% v/w (for labeled substrate) acrylamide−8 M urea gels. The substrate strand contained a 2′-deoxy substitution, nucleotide C17. Significant protection was observed at G5−A9 in the ribozyme and C17−U1.2 in the substrate strand. These sites are indicated by black dots and are referred to by the residue number to the right of each panel. The rightmost lane of panel A contains a 2′-deoxy substitution at position G5 of the ribozyme strand. Open spheres indicate sites that are protected in ribozyme−substrate complexes in Mg^{2+}, but not in substrate or ribozyme alone or in the absence of Mg^{2+}. Alkali hydrolysis (Alk) and ribonuclease T1 (T1) digested control lanes are to the left of each panel. Note that the identity of each band on the Fe(II)-EDTA ladders is actually one nucleotide below the corresponding band on partial ribonuclease T1 and alkali hydrolysis ladders.

Mg^{2+} experiments. For Li^+ titrations, reactions were stopped by adding 300 μL of ethanol, 50 μL of 3 M sodium acetate, and 2.5 μL of 10 μg/μL tRNA and then were allowed to precipitate for 1 h at −70 °C. RNA pellets were recovered by centrifugation at 13000 rpm in a benchtop microfuge and resuspended in 20 μL of gel addition buffer. The following buffers were used for reactions performed at pHs other than 7: pH 6−6.5, Mes; pH 8−9, Tris. Time-resolved footprinting was performed exactly as described previously with no modifications (*41*).

Catalytic Assays. For single-turnover cleavage assays an RNA solution composed of a trace concentration (<10 nM) of 5′-^{32}P-end-labeled substrate, a saturating concentration of ribozyme (HH16, 1 μM; HHα1 and RNA, 6 and 5 μM), strand, and 25 mM sodium cacodylate, pH 7, was incubated for 20 min at 37 °C. The solution was then equilibrated to 25 °C for 5 min. Cleavage reactions were initiated by adding 1 volume of a cation solution (1.5 volumes for reactions in Li^+), equilibrated at 25 °C, to the RNA mix. Aliquots were quenched at specific time points into 10 volumes of 95% (v/v) formamide, 20 mM EDTA, 0.02% (w/v) bromophenol blue, and 0.02% (w/v) xylene cyanol, on ice. Zero time points were generated by prequenching cation and RNA solutions. No detectable amount of cleavage in the zero time points was observed. Cleavage kinetics were quantified by fitting the cleaved fraction vs time plots using Marquardt−Levenberg nonlinear least-squares regression to the exponential association equation $y = y_0 + A(1 - e^{-t/\tau})$ with Microcal Origin 4.1 software.

RESULTS

Our initial footprinting studies were performed with a two-strand HH16 ribozyme construct (*42*), containing shortened stems 1 and 3 (Figure 1). A 2′-deoxy substitution at nucleotide C17 was incorporated in order to prevent cleavage of the substrate. Fe(II)-EDTA footprinting of this construct as a function of added Mg^{2+} resulted in the visualization of several sites of backbone protection (Figure 2A). Sites of protection were verified by quantitative radioimaging analysis and ranged in magnitude from 30% to 55% protection. We did not observe protection of any sites with either strand alone at 20 mM Mg^{2+} after 30 min of incubation (Figure 2B). Thus, protection of the backbone sites in Mg^{2+} requires assembly of the full ribozyme−substrate complex. The sites of protection identified in HH16, G5−A9 and C17−U1.2, are clustered around the densely packed three-helix junction. Hydroxyl radical-mediated cleavage of residues close to the 3′-terminus of HH16 was difficult to quantify due to higher background at those positions on the gel. Overall, the location of protections provided some confidence that they might result from a specific tertiary structure along the native folding pathway for the ribozyme.

To determine the sequence specificity for the appearance of this collection of solvent-protected sites, we analyzed two other hammerhead constructs with different connectivities and noncore sequences, HHα1 and RNA 6 (*43*, *44*; Figure 3). These two constructs displayed solvent-protected surfaces identical to those of HH16 with one exception. Protection of the ribose at position 15.3 is clearly observed in these constructs. We have attempted to quantify protection of

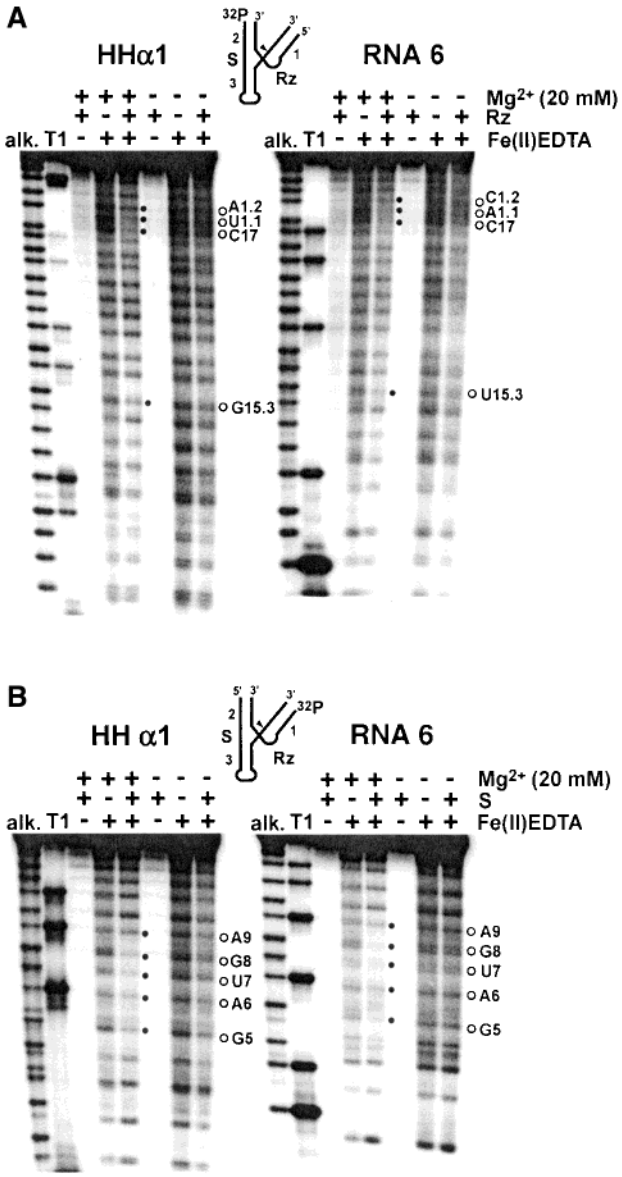

FIGURE 3: Partial hydroxyl radical protection of the Rz (A) and S (B) strands of HHα1 and RNA 6 hammerhead complexes. The solid spheres indicate sites of solvent protection. Open spheres are used to show sites that are not protected in the absence of S or Rz stands or Mg^{2+}. Residues U16.1−1.2, G5−A9, and 15.3 are protected in both constructs.

G15.3 in HH16 constructs without success, possibly due to the high background at its location on the gel. The inclusion of 15.3 among the solvent-protected residues is very significant since, in the crystal structures of the hammerhead, domain 1 approaches this region of stem 3 (*13*, *14*). This represents a highly specific correspondence between the crystal structures and this hydroxyl radical footprinting solvent-based assay system.

At least three hypotheses may be invoked to account for our results with respect to the numbers of structures involved and the degree of solvent accessibility in each structure. (1) The low level of solvent protection (≤2-fold) that we have observed at these locations may be due to the fact that more than one different partially protected structure exists under these conditions. (*2*) A single highly protected structure is present in solution, but it accounts for only approximately 50% of the molecules. (*3*) The ribozymes in solution are

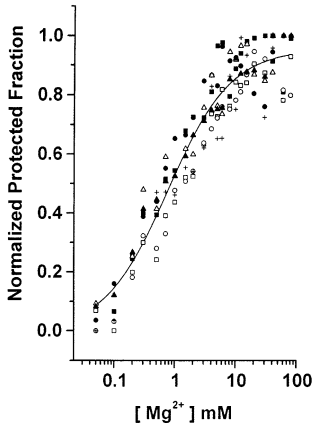

FIGURE 4: The Mg^{2+} dependence for hydroxyl radical protection of HHα1 displays little site to site variation. HHα1 complexes were treated with varying concentrations of Mg^{2+} in 25 mM sodium cacodylate, pH 7, buffer and then treated with hydroxyl radicals. The level of protection at C17 (■), U1.1 (□), A1.2 (●), A6 (○), U7 (▲), G8 (△), and C15.3 (+) was quantified using a Bio-Rad radioimaging system. The results are the average of at least two independent experiments. The number of counts for each lane was corrected for loading and hydroxyl radical-mediated cleavage by comparing the counts at nonprotected positions 16.3, 1.4, 10.2, and 3. The protected fraction was calculated from the equation $f = 1 - (C_x/C_0)$, where C_0 and C_x are the number of corrected counts for a single residue at 0 and x mM Mg^{2+}. Normalization was carried out so that the maximal protection observed in each experiment was valued at 1. The levels of protection observed at each site are listed in Figure 6. The dependence of rate constants and protection amplitudes on the Mg^{2+} concentration was fitted for all seven data sets simultaneously to the cooperative binding equation $f = f_{max}\text{-}([Mg^{2+}]^n/([Mg^{2+}]^n + (K_d^{Mg})^n))$ to yield an apparent dissociation constant K_d^{Mg} of 0.77 ± 0.06 mM and a cooperativity coefficient, n, of 0.84 ± 0.05.

structurally uniform but possess a structure in which the core is only partially protected from solvent. If more than one structure gives rise to the protections that we observe, it is unlikely that all would have identical cation requirements. To test this, we incubated the ribozyme over a broad range of Mg^{2+} and Li^+ concentrations (Figure 4). All sites on HHα1 were protected with very similar apparent K_d values for Mg^{2+} (Figure 4) and Li^+ (~300 mM; data not shown). Thus, we believe that a single structure gives rise to the observed pattern of hydroxyl radical protections. Furthermore, the value for Mg^{2+} dependence is in the same range that has been previously observed for global structural changes as monitored by FRET and 2-aminopurine fluorescence changes (*16*, *26*).

Since global folding of the hammerhead in Mg^{2+}-containing solutions can be altered by 2′-deoxy substitution of the essential residue G5 (*21*, *45*), we examined this single atom substitution using the hydroxyl radical footprinting method. Our data show that folding of the ribozyme−substrate complex into a solvent-protected form is not observed in complexes with this substitution (Figures 2A and 5). This result strongly suggests that the structure that we describe here is similar or identical to the structure that has been monitored in solution experiments by other laboratories.

If the structure that we observe is on the native folding pathway, under all conditions, the rate of folding should be greater than or equal to the rate of catalysis. The rate of acquisition of this folded structure was, therefore, analyzed

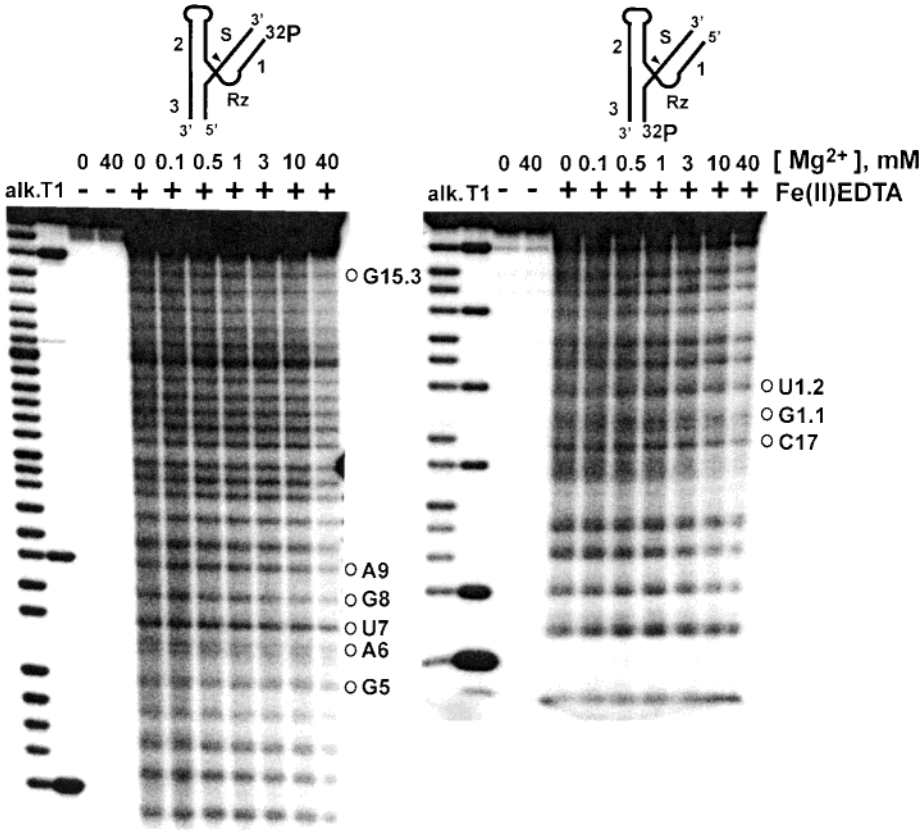

FIGURE 5: Folding of 2′-deoxy G5-substituted (dG5) HH16 ribozymes in Mg^{2+} does not result in solvent protection of the hammerhead motif. End-labeled Rz (left panel) and S (right panel) were incubated in 25 mM sodium cacodylate, pH 7, and Mg^{2+} at the concentrations indicated and then treated with Fe(II)-EDTA solutions or left untreated. Sites of protection in unsubstituted ribozymes in Mg^{2+} that are not observed in dG5 HH16 complexes are indicated by open spheres at the right of each panel.

by time-resolved footprinting (*38*, *41*). In these experiments, hammerhead RNA was mixed with Mg^{2+} and allowed to incubate for a period of time before the addition of the reagents that generate hydroxyl radicals. The results of this experiment showed that, under all conditions tested, approximately 50% of maximal folding occurred during the 3 s dead time of the experiment where Mg^{2+} and hydroxyl radical-generating reagents were added simultaneously (data not shown). Therefore, we are unable to describe the folding rate more accurately than to set its lower limit at the fastest measurement possible with this system, 8 min^{-1}. The single-turnover rate of catalysis was measured between pH 6 and pH 8.5, and our data are similar to studies finding a roughly log-linear dependence of cleavage rate on pH (*8*). In addition, we report that we found no significant difference in the magnitude of cleavage or protection as a function of pH over this range. Above pH 8.5 we were unable to measure the rate of cleavage accurately by hand for HH16 at 25 °C. Under all conditions where both folding and catalysis could be measured, however, we found that folding was faster. The difference between folding and cleavage rates was particularly large at low pH. These results are consistent with the hypothesis that this folded structure is on the native folding pathway.

We were also concerned that the 2′-deoxy substitution of C17 could possibly influence the pattern of solvent protections. Deprotonation of the 2′-oxygen of C17 is postulated to promote a conformational change at the active site of the ribozyme, which leads to catalysis (*11*). We have not been able to investigate this phenomenon in our system since the very rapid cleavage of substrate at the very alkaline conditions needed to deprotonate this functional group makes footprinting impossible. The slow cleavage rate at pH 6 for HH16 (k_{cleave} = 0.032 min^{-1}), however, enabled us to employ hydroxyl radical footprinting on ribozyme with a saturating concentration of a cleavable, all ribose substrate. Under these conditions, solvent protection of the ribozyme strand, residues G5−A9, is unimpaired relative to those obtained with a 2′-deoxy-modified substrate (data not shown). Thus, inclusion of this single atom substitution does not effect global folding. This is consistent with previous reports showing that when RNA or DNA substrates are employed, nearly identical ribozyme folding results are obtained (*13*, *14*, *46*, *47*).

Figure 6 summarizes the hydroxyl radical protection data from these experiments. To examine the correspondence of this structure with known high-resolution forms further, we calculated the solvent accessibility of the C4′ atom on two crystal structures (*14*, *47*) and superimposed our experimental data on this plot (Figure 6B). The data sets correspond quite well. We observed as partially protected from hydroxyl radical attack several residues at the three-stem junction with reduced solvent accessibility in the crystal structures, G5, A6, G8, and C17. Most striking is the reduction in accessibility of G15.3 predicted by both structures and by our data. In the crystal structures the U-turn motif approaches stem 3 at this site (Figure 6C). This indicates that the structural basis of this protection is the conformation of the U-turn motif at the base of helix 1. In addition, however, four residues that are protected in our experiments, U7, A9, A1.1, and C1.2,

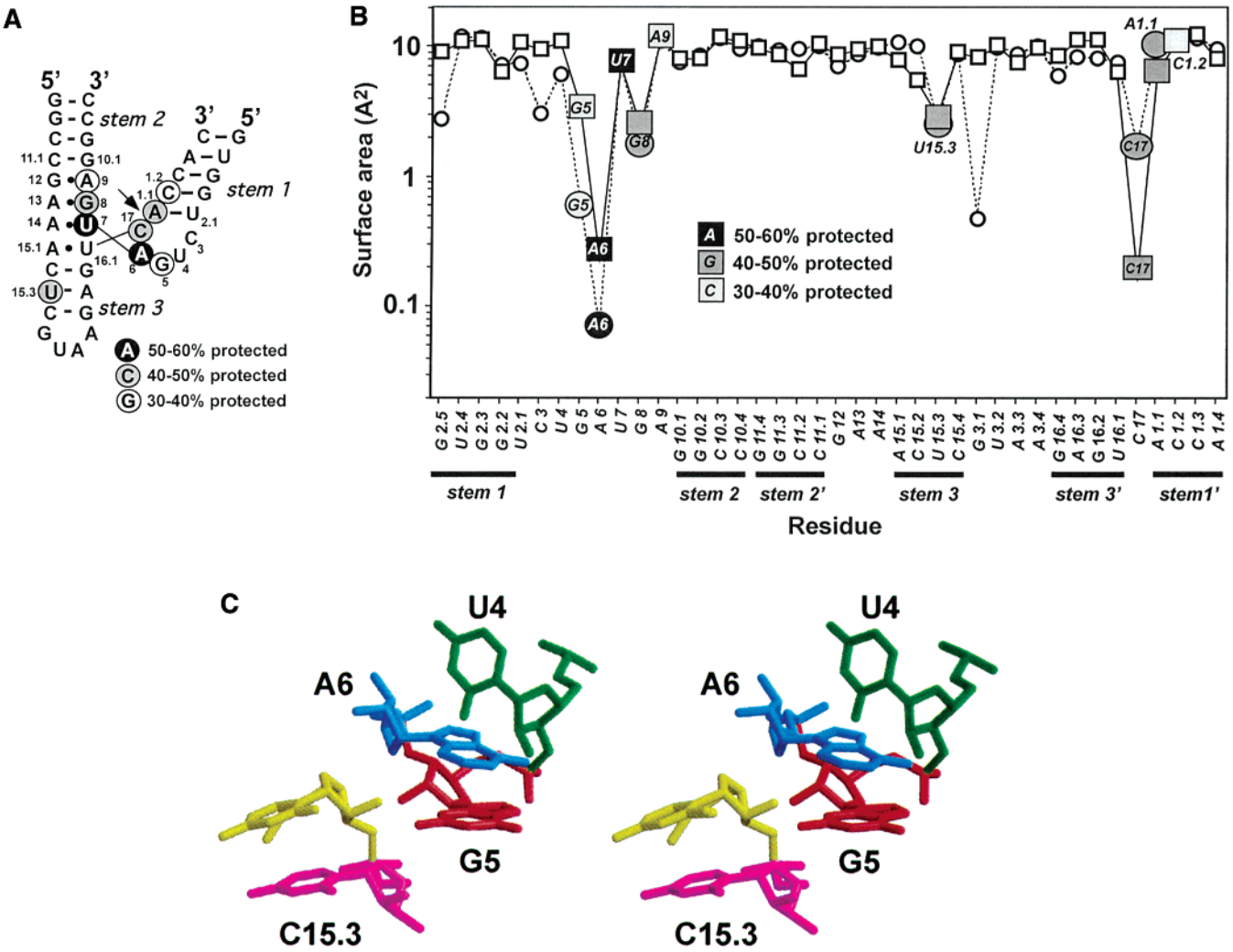

FIGURE 6: (A) Summary of solvent protections induced by cation-dependent conformational changes. The secondary structure of RNA 6 is shown with spheres indicating sites and average magnitude of protections. (B) Comparison of observed solvent protection with solvent accessibilities calculated from two crystal structures [Scott et al. (*14*; spheres) and Murray et al. (*47*; squares)]. Solvent accessibility was calculated with the solvation module of Accelrys Insight II software, assuming the standard solvent diameter of 1.4 Å, and plotted against the linear sequence of residues. Solvent protection from hydroxyl radicals was then superimposed on this plot by shading of enlarged squares and circles. An intermolecular contact between the GUAA tetraloop and its receptor in helix 1 is responsible for the partial solvent inaccessibility of G3.1. (C) Stereo closeup of a portion of a hammerhead crystal structure (*47*) showing close approach of residues in domain 1, U4 (green), G5 (red), and A6 (blue), and residues 15.2 (yellow) and 15.3 (magenta) in stem 3. The picture was rendered with Molscript software.

are highly solvent accessible in the X-ray structures. These residues lie in a pocket between stem 1 and domain 2. If these two structural elements were shifted slightly toward one another, it is conceivable that these additional residues would become solvent protected without dramatically altering the crystal structure.

Metal ions are important for both folding and catalysis in the hammerhead. We tested several mono-, di-, and multivalent cations for their ability to promote folding of the hammerhead. Mn^{2+}, Sr^{2+}, Ca^{2+}, and Co^{2+} were all able to stimulate folding of the hammerhead into the solvent-protected form. In addition, Na^{+} and Li^{+} were able to promote the formation of this structure (data not shown). The magnitudes of backbone protections in all mono- and divalent cations tested were close to or slightly exceeded those observed in Mg^{2+}, and there was no change in the identity of protected sites. In contrast, cobalt(III) hexaammine was able to promote only weak protection, approximately 50% of Mg^{2+}-induced protection at all sites. Footprinting in the presence of cobalt(III) hexaammine is limited to concentrations of 10 mM or less due to quenching of hydroxyl radicals. In 10 mM cobalt(III) hexaammine the cleavage rate of the hammerhead at pH 7 is 0.015 min^{-1}, which is 15-fold slower than that observed at the same concentration of Mg^{2+} (data not shown).

We were also interested in determining the relative cation concentration requirements for catalysis and folding. Folding extents and single-turnover cleavage reaction rates were titrated with respect to Mg^{2+} and Li^{+} concentrations on HH16 under nearly identical solution conditions (Figure 7). The apparent K_d^{Mg} of 20.7 ± 2.3 mM for cleavage is 20-fold greater than that required for folding, K_d^{Mg} = 1.1 ± 0.12 mM. This differential was constant for all three ribozyme constructs even though their cleavage rates vary over ~200-fold at pH 7 (data not shown), suggesting that a common structural change in the conserved core of the ribozyme is required for full catalytic activity.

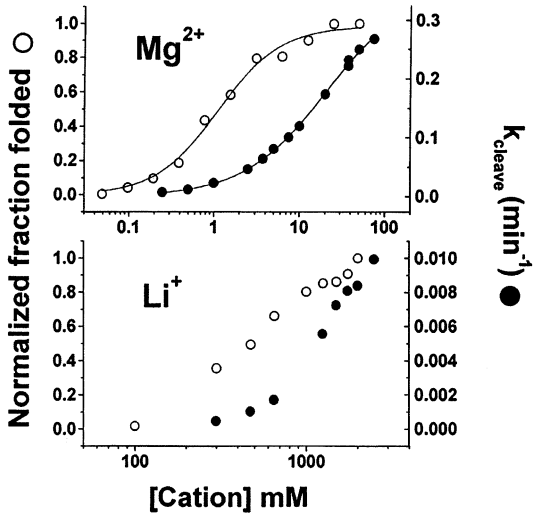

FIGURE 7: Cation requirements for catalysis are higher than for folding to the ground state configuration. HH16 ribozyme−substrate complexes were incubated in 25 mM sodium cacodylate, pH 7, over a range of Mg^{2+} or Li^+ concentrations and then treated with hydroxyl radical-generating reagents. Normalized protection at position C17 was quantified using a Bio-Rad phosporimaging system and plotted as a function of the cation concentration. The average of at least two determinations is reported. Values were normalized relative to the level of protection at the single concentration at which maximal protection was observed. Cleavage assays were carried out as described in Materials and Methods. Cleavage and folding assays were constituted identically with two exceptions. First, for protection assays a noncleavable substrate analogue (2′-deoxy C17) was employed. Second, folding was assayed by addition of hydroxyl radical-generating reagents, which made up 20% of the experimental solution volume. These differences cannot account for the significant differences in folding and catalytic cation dependencies. The apparent dissociation constant, K_d^{Mg}, and cooperativity coefficients, n, for folding and cleavage, 1.1 ± 0.1 mM, $n = 1.2$ and 20.7 ± 2.3 mM, $n = 0.9$, respectively, were calculated using the cooperative binding equation from Figure 4.

DISCUSSION

Our data support the view that in Mg^{2+}-containing solutions the hammerhead ribozyme predominantly resides in a global tertiary structure similar or identical to that represented by the crystal structures. First, the Mg^{2+} dependence for the formation of this structure is very similar to that observed by FRET analysis, which defines the y-shape or so-called I/II motif seen in crystal structures (*16*). Second, 2′-deoxy substitution of G5 results in a loss of the ability of the ribozyme to fold into a solvent-protected form and also blocks formation of the I/II motif in FRET analysis (*45*). Third, the sites of hydroxyl radical protection on the ribozyme−substrate complex fit well with the computed solvent accessibility of the backbone from two crystal forms. Furthermore, the concurrence of the two data sets extends from the conserved core and cleavage site sequences to protection of a nonconserved residue in helix III, U15.3 in RNA 6. The positioning of the residues in domain 1 in published crystal structures is responsible for the calculated protection of U15.3, and the fact that we observed solvent protection at that site provides very strong evidence that the crystal form is present to a significant level in solution.

In our experiments, partial protection extends to adjacent residues not predicted to be protected from the crystal forms. For example, U7 is solvent accessible in the two crystal structures, but our data show that this residue is significantly protected in solution. This suggests that while the overall geometry observed in crystal form and in our experiments is likely to be the same, the motif forms a somewhat more compact form in the wide range of cations and pHs that we have explored. The observation that single atom substitution of G5 (2′-deoxy) eliminates the formation of the solvent-protected hammerhead, coupled with the similarities between the apparent K_d^{Mg} of formation between our structure and the structure reported by Lilley and co-workers, suggests that the two forms are one and the same. An additional conformational change, which has been observed at submillimolar concentrations of Mg^{2+}, represents the formation of domain 2 (*16*). Evidence of this structure has not been observed in the present study, probably due to the fact that it does not protect specific residues from attack by hydroxyl radicals.

Though it is unlikely that our data result from footprinting greater than one structure, we have not been able to quantify the abundance of this structure in solution. Application of time-resolved FRET (trFRET) methodology, which we have previously used to define the abundance of various conformers of the hairpin ribozyme in solution (*48*), will be of value in making these calculations since an unambiguous FRET signal is indicative of this hammerhead structure. Since the rate of folding is much faster than catalysis, it will be difficult to determine if this form is on the native folding pathway for the hammerhead, a problem we previously encountered with the hairpin ribozyme (*49*). Single molecule analysis of the hairpin was recently employed to show that a known conformational change, for which a hydroxyl radical footprint has been determined, leads directly to ribozyme-catalyzed strand scission (*50*). This approach may also be applicable to the hammerhead system.

Our results with different hammerhead sequences allow us to suggest a role for nonconserved residues of catalytic significance. While the identity of the 2.1−1.1 base pair is not highly conserved in natural phylogenies of the hammerhead motif, this base pair has been shown to be important for catalytic activity (*51*). A HH16 variant with a U1.1−A2.1 base pair (HH16.43) has a cleavage rate close to 10-fold faster than HH16 (*51*). Cleavage kinetics carried out on HH16, HHα1, and RNA 6 show a very large range of activities (*51*; K. J. Hampel and J. M. Burke, unpublished observations), and all have different 1.1−2.1 base pairs. HHα1 ($k_{cleave} = 2.33$ min^{-1}, pH 7, 10 mM Mg^{2+}) is approximately 20-fold faster than HH16, which in turn is approximately 10-fold faster than RNA 6. This 200-fold range in activities between the three hammerheads cannot be attributed to differences in formation of the ground state structure, since we observed similar protection magnitudes and patterns for these constructs. Therefore, we suggest that the catalytic effect of this base pair is manifested at a step after formation of this global fold, possibly during formation of the transition state structure. Although the formation of the solvent-protected structure is not catalytically rate limiting for these constructs, we cannot rule out the possibility that the ground state structures for different constructs retain subtle differences, not detectable by hydroxyl radical footprinting, that affect the catalytic rate.

Although specific metal ion binding sites have been resolved in hammerhead crystal forms (*13*, *14*, *23*, *52*, *53*) and by NMR methods (*54*, *55*), our data suggest that many

different monovalent and divalent cations are equally capable of promoting formation of the solvent-protected form. This is consistent with published data on the hammerhead showing that several different cations are capable of promoting the formation of an active complex (*8*). Some cations, however, clearly support greater activity than others. For example, Mg^{2+} is able to support catalysis at rates which are 5−10-fold greater than those observed for Li^+ (*24*, *25*; Figure 7). It has been proposed by Herschlag and co-workers that this is due to the unique ability of specific divalent cations to promote folding to the transition state structure and/or to directly assist in the chemistry of the transesterification reaction (*25*). This hypothesis is based, in part, on Cd^{2+} rescue of phosphorothioate modifications, indicating that one of the divalent metal ions seen in the crystal structures, bound to the *pro-*R_p phosphate O of A9 and the N7 of G10.1 (P9/10.1), acquires an additional ligand that is functional in the transition state, the *pro-*R_p phosphate O of the cleavage site phosphodiester (*27*). Bridging of P9/10.1 and the cleavage sites represents a significant change in structure from the crystal form and has been challenged on the basis of modeling studies (*56*). Li^+ is not able to rescue either phosphorothioate modification (*25*). This may explain why Li^+ cannot support full cleavage activity in the absence of Mg^{2+}. Nevertheless, our data demonstrate that Li^+ is able to mediate folding of the ribozyme to the same extent as has been observed for Mg^{2+}.

Our data show that the apparent K_d values for Mg^{2+} and Li^+ for folding are lower than those for catalysis, which is consistent with a requirement for cation-dependent conformational change by the ribozyme required to achieve the active structure, but with generalized cation specificity. It is less likely that the additional cation requirement for catalysis is due to binding of a catalytic cation to a preformed active site. Very different cations such as Li^+ and Mg^{2+} are unlikely to find similar binding pockets at the active site and then assist the chemistry of the reaction in the same way. Our data extend previous results from NMR studies that have identified metal ion binding sites with distinct binding affinities (*55*). The generality of the increased cation requirement for folding to the transition state may be rationalized as follows. The proposed linkage between the P9/10 and cleavage sites (*27*) would result in significant compaction of the ribozyme relative to the crystal form or ground state. Cations are generally well suited to assist in this process since they are able to counteract the increase in negative charge density from the RNA backbone. The reason Mg^{2+} promotes greater cleavage activity than Li^+ or multivalent cations such as cobalt(III) hexaammine may be, as has been suggested by Herschlag and co-workers, that Mg^{2+} optimally folds the ribozyme's active site (*25*).

While our data support the hypothesis of a conformational change between the ground and transition states, we were unable to detect any difference between footprints on a ribozyme with a cleavable or noncleavable substrate. On the surface, these data support previous crystallographic data for the RNA 6 hammerhead which shows only a local, small-scale Co^{2+}-induced conformational change from the ground state, in which the attacking nucleophile is not properly aligned for attack of the phosphorus, to a form where the nucleophile has attained an in-line attack geometry with respect to the scissile phosphodiester (*47*). However, the crystallographic result has been criticized as the conformational change has a rate that is slower than cleavage of the substrate in the crystals (*27*). It has further been suggested that the equilibrium between the ground and transition state structures favors the ground state (*25*). In this case the hydroxyl radical footprints of the catalytically active complex at pH 6 would only be expected to report on the most abundant species, the ground state structure.

ACKNOWLEDGMENT

The authors thank Dominic Lambert for rendering the image in Figure 6 and making the solvent accessibility calculations and Anne MacLeod for assistance in preparing the manuscript.

REFERENCES

1. Buzayan, J. M., Gerlach, W. L., and Breuning, G. (1986) Non-enzymatic cleavage and ligation of RNAs complementary to a plant virus satellite RNA, *Nature 323*, 349−353.
2. Epstein, L. M., and Gall, J. G. (1987) Self-cleaving transcripts of satellite DNA from the newt, *Cell 48*, 535−543.
3. Ferbeyre, G., Smith, J. M., and Cedergren, R. (1998) Schistosome satellite DNA encodes active hammerhead ribozymes, *Mol. Cell. Biol. 18*, 3880−3888.
4. Ferbeyre, G., Bourdeau, V., Pageau, M., Miramontes, P., and Cedergren, R. (2000) Distribution of hammerhead and hammerhead-like RNA motifs through the GenBank, *Genome Res. 10*, 1011−1019.
5. Salehi-Ashtiani, K., and Szostak, J. W. (2001) *In vitro* evolution suggests multiple origins for the hammerhead ribozyme, *Nature 414*, 82−84.
6. Hutchins, C. J., Rathjen, P. D., Forster, A. C., and Symons, R. H. (1986) Self-cleavage of plus and minus RNA transcripts of avocado sunblotch viroid, *Nucleic Acids Res. 14*, 3627−3640.
7. Forster, A. C., and Symons, R. H. (1987) Self-cleavage of plus and minus RNAs of a virusoid and a structural model for the active sites, *Cell 49*, 211−220.
8. Dahm, S. C., Derrick, W. B., and Uhlenbeck, O. C. (1993) Evidence for the role of solvated metal hydroxide in the hammerhead cleavage mechanism, *Biochemistry 32*, 13040−13045.
9. Hertel, K. J., and Uhlenbeck, O. C. (1995) The internal equilibrium of the hammerhead ribozyme reaction, *Biochemistry 34*, 1744−1749.
10. Stage-Zimmermann, T. K., and Uhlenbeck, O. C. (1998) Hammerhead ribozyme kinetics, *RNA 4*, 875−889.
11. Murray, J. B., Dunham, C. M., and Scott, W. G. (2002) A pH-dependent conformational change, rather than the chemical step, appears to be rate-limiting in the hammerhead ribozyme cleavage reaction, *J. Mol. Biol. 315*, 121−130.
12. Ruffner, D. E., Stormo, G. D., and Uhlenbeck, O. C. (1990) Sequence requirements of the hammerhead RNA self-cleavage reaction, *Biochemistry 29*, 10695−10702.
13. Pley, H. W., Flaherty, K. M., and McKay, D. B. (1994) Three-dimensional structure of a hammerhead ribozyme, *Nature 372*, 68−74.
14. Scott, W. G., Finch, J. T., and Klug, A. (1995) The crystal structure of an all-RNA hammerhead ribozyme: a proposed mechanism for RNA catalytic cleavage, *Cell 81*, 991−1002.
15. Bassi, G. S., Mollegaard, N. E., Murchie, A. I., von Kitzing, E., and Lilley, D. M. (1995) Ionic interactions and the global conformations of the hammerhead ribozyme, *Nat. Struct. Biol. 2*, 45−55.
16. Bassi, G. S., Murchie, A. I., Walter, F., Clegg, R. M., and Lilley, D. M. (1997) Ion-induced folding of the hammerhead ribozyme: a fluorescence resonance energy transfer study, *EMBO J. 16*, 7481−7489.
17. Sigurdsson, S. T., Tuschl, T., and Eckstein, F. (1995) Probing RNA tertiary structure: interhelical crosslinking of the hammerhead ribozyme, *RNA 1*, 575−583.
18. Stage-Zimmermann, T. K., and Uhlenbeck, O. C. (2001) A covalent cross-link converts the hammerhead ribozyme from a ribonuclease to an RNA ligase, *Nat. Struct. Biol. 8*, 863−867.

19. Amiri, K. M., and Hagerman, P. J. (1994) Global conformation of a self-cleaving hammerhead RNA, *Biochemistry 33*, 13172−13177.
20. Fu, D. J., and McLaughlin, L. W. (1992) Importance of specific purine amino and hydroxyl groups for efficient cleavage by a hammerhead ribozyme, *Proc. Natl. Acad. Sci. U.S.A. 89*, 3985−3989.
21. Bassi, G. S., Murchie, A. I., and Lilley, D. M. (1996) The ion-induced folding of the hammerhead ribozyme: core sequence changes that perturb folding into the active conformation, *RNA 2*, 756−768.
22. Dahm, S. C., and Uhlenbeck, O. C. (1991) Role of divalent metal ions in the hammerhead RNA cleavage reaction, *Biochemistry 30*, 9464−9469.
23. Murray, J. B., Seyhan, A. A., Walter, N. G., Burke, J. M., and Scott, W. G. (1998) The hammerhead, hairpin and VS ribozymes are catalytically proficient in monovalent cations alone, *Chem. Biol. 5*, 587−595.
24. Curtis, E. A., and Bartel, D. P. (2001) The hammerhead cleavage reaction in monovalent cations, *RNA 7*, 546−552.
25. O'Rear, J. L., Wang, S., Feig, A. L., Beigelman, L., Uhlenbeck, O. C., and Herschlag, D. (2001) Comparison of the hammerhead cleavage reactions stimulated by monovalent and divalent cations, *RNA 7*, 537−545.
26. Menger, M., Tuschl, T., Eckstein, F., and Porschke, D. (1996) Mg^{2+}-dependent conformational changes in the hammerhead ribozyme, *Biochemistry 35*, 14710−14716.
27. Wang, S., Karbstein, K., Peracchi, A., Beigelman, L., and Herschlag, D. (1999) Identification of the hammerhead ribozyme metal ion binding site responsible for rescue of the deleterious effect of a cleavage site phosphorothioate, *Biochemistry 38*, 14363−14378.
28. Russell, R., and Herschlag, D. (1999) New pathways in folding of the Tetrahymena group I RNA enzyme, *J. Mol. Biol. 291*, 1155−1167.
29. Woisard, A., Fourrey, J. L., and Favre, A. (1994) Multiple folded conformations of a hammerhead ribozyme domain under cleavage conditions, *J. Mol. Biol. 239*, 366−370.
30. Wang, L., and Ruffner, D. E. (1997) An ultraviolet crosslink in the hammerhead ribozyme dependent on 2-thiocytidine or 4-thiouridine substitution, *Nucleic Acids Res. 25*, 4355−4361.
31. Galas, D. J., and Schmitz, A. (1978) DNAse foot-printing: a simple method for the detection of protein-DNA binding specificity, *Nucleic Acids Res. 5*, 3157−3170.
32. Ehresmann, C., Baudin, F., Mougel, M., Romby, P., Ebel, J. P., and Ehresmann, B. (1987) Probing the structure of RNAs in solution, *Nucleic Acids Res. 15*, 9109−9128.
33. Krol, A., and Carbon, P. (1989) A guide for probing native small nuclear RNA and ribonucleoprotein structures, *Methods Enzymol. 180*, 212−227.
34. Sclavi, B., Sullivan, M., Chance, M. R., Brenowitz, M., and Woodson, S. A. (1998) RNA folding at millisecond intervals by synchrotron hydroxyl radical foot-printing, *Science 279*, 1940−1943.
35. Rose, M. A., and Weeks, K. M. (2001) Visualizing induced fit in early assembly of the human signal recognition particle, *Nat. Struct. Biol. 8*, 515−520.
36. Latham, J. A., and Cech, T. R. (1989) Defining the inside and outside of a catalytic RNA molecule, *Science 245*, 276−282.
37. Hampel, K. J., Walter, N. G., and Burke, J. M. (1998) The solvent-protected core of the hairpin ribozyme-substrate complex, *Biochemistry 37*, 14672−14682.
38. Hampel, K. J., and Burke, J. M. (2001) A conformational change in the "loop E-like" motif of the hairpin ribozyme is coincidental with domain docking and is essential for catalysis, *Biochemistry 40*, 3723−3729.
39. Walter, N. G., Yang, N., and Burke, J. M. (2000) Probing nonselective cation binding in the hairpin ribozyme with Tb(III), *J. Mol. Biol. 298*, 539−555.
40. Butcher, S. E., and Burke, J. M. (1994) A photo-cross-linkable tertiary structure motif found in functionally distinct RNA molecules is essential for catalytic function of the hairpin ribozyme, *Biochemistry 33*, 992−999.
41. Hampel, K. J., and Burke, J. M. (2001) Time-resolved hydroxyl-radical foot-printing of RNA using Fe(II)-EDTA, *Methods 23*, 233−239.
42. Hertel, K. J., Herschlag, D., and Uhlenbeck, O. C. (1994) A kinetic and thermodynamic framework for the hammerhead ribozyme reaction, *Biochemistry 33*, 3374−3385.
43. Clouet-D'Orval, B., and Uhlenbeck, O. C. (1996) Kinetic characterization of two I/II format hammerhead ribozymes, *RNA 2*, 483−491.
44. Scott, W. G., Finch, J. T., Grenfell, R., Fogg, J., Smith, T., Gait, M. J., and Klug, A. (1995) Rapid crystallization of chemically synthesized hammerhead RNAs using a double screening procedure, *J. Mol. Biol. 250*, 327−332.
45. Bassi, G. S., Mollegaard, N. E., Murchie, A. I., and Lilley, D. M. (1999) RNA folding and misfolding of the hammerhead ribozyme, *Biochemistry 38*, 3345−3354.
46. Amiri, K. M., and Hagerman, P. J. (1996) The global conformation of an active hammerhead RNA during the process of self-cleavage, *J. Mol. Biol. 261*, 125−134.
47. Murray, J. B., Terwey, D. P., Maloney, L., Karpeisky, A., Usman, N., Beigelman, L., and Scott, W. G. (1998) The structural basis of hammerhead ribozyme self-cleavage, *Cell 92*, 665−673.
48. Walter, N. G., Burke, J. M., and Millar, D. P. (1999) Stability of hairpin ribozyme tertiary structure is governed by the interdomain junction, *Nat. Struct. Biol. 6*, 544−549.
49. Walter, N. G., Hampel, K. J., Brown, K. M., and Burke, J. M. (1998) Tertiary structure formation in the hairpin ribozyme monitored by fluorescence resonance energy transfer, *EMBO J. 17*, 2378−2391.
50. Zhuang, X., Kim, H., Pereira, M. J., Babcock, H. P., Walter, N. G., and Chu, S. (2002) Correlating structural dynamics and function in single ribozyme molecules, *Science 296*, 1473−1476.
51. Clouet-d'Orval, B., and Uhlenbeck, O. C. (1997) Hammerhead ribozymes with a faster cleavage rate, *Biochemistry 36*, 9087−9092.
52. Scott, W. G., Murray, J. B., Arnold, J. R. P., Stoddard, B. L., and Klug, A. (1996) Capturing the structure of a catalytic RNA intermediate: The hammerhead ribozyme, *Science 274*, 2065−2069.
53. Feig, A. L., Scott, W. G., and Uhlenbeck, O. C. (1998) Inhibition of the hammerhead ribozyme cleavage reaction by site-specific binding of Tb, *Science 279*, 81−84.
54. Hansen, M. R., Simorre, J. P., Hanson, P., Mokler, V., Bellon, L., Beigelman, L., and Pardi, A. (1999) Identification and characterization of a novel high affinity metal-binding site in the hammerhead ribozyme, *RNA 5*, 1099−1104.
55. Maderia, M., Hunsicker, L. M., and DeRose, V. J. (2000) Metal-phosphate interactions in the hammerhead ribozyme observed by 31P NMR and phosphorothioate substitutions, *Biochemistry 39*, 12113−12120.
56. Murray, J. B., and Scott, W. G. (2000) Does a single metal ion bridge the A-9 and scissile phosphate groups in the catalytically active hammerhead ribozyme structure?, *J. Mol. Biol. 296*, 33−41.
57. Hertel, K. J., Pardi, A., Uhlenbeck, O. C., Koizumi, M., Ohtsuka, E., Uesugi, S., Cedergren, R., Eckstein, F., Gerlach, W. L., Hodgson, R., and Symons, R. H. (1992) Numbering system for the hammerhead, *Nucleic Acids Res. 20*, 3252.

BI020659C